Hydrometeorological dataset of West Siberian boreal peatland: a 10-year records from the Mukhrino field station

Egor Dyukarev[1,2], Nina Filippova[1], Dmitriy Karpov[1], Nikolay Shnyrev[3], Eugeniy Zarov[1], Ilya Filippov[1], Nadezhda Voropay[2,4], Vitaly Avilov[5], Arseniy Artamonov[6], Elena Lapshina[1]

Supplementary materials

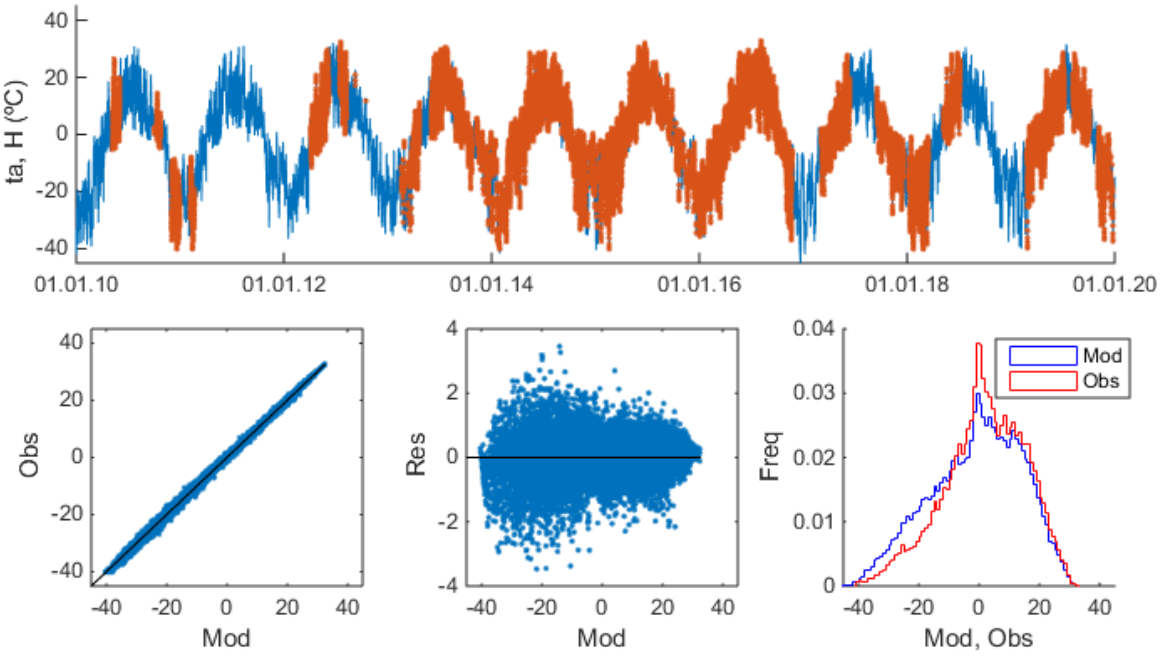

Figure S1. Air temperature measured at the hollow at the Mukhrino field station.

Legend. Top panel: 1 – observations, 2 – gap-filling model data. Bottom panel: relations of observed and model data (left), model residuals vs model data (centre), frequency distributions for model and observed data (right).

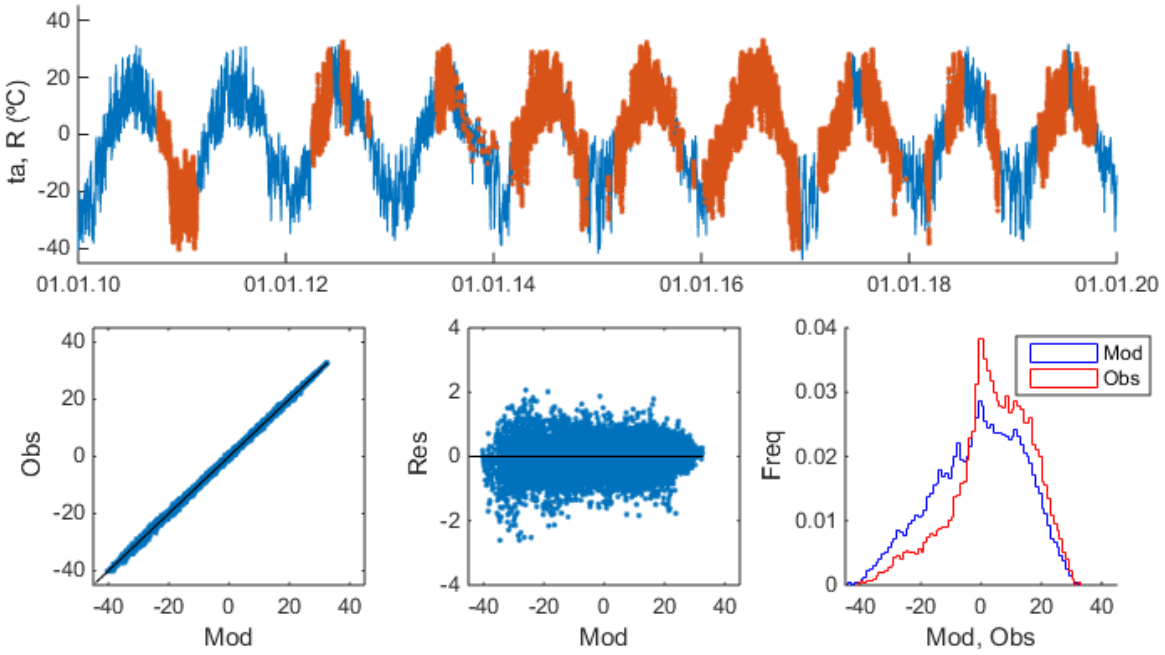

Figure S2. Air temperature at the ridge at the MFS. See legend at Fig. S1.

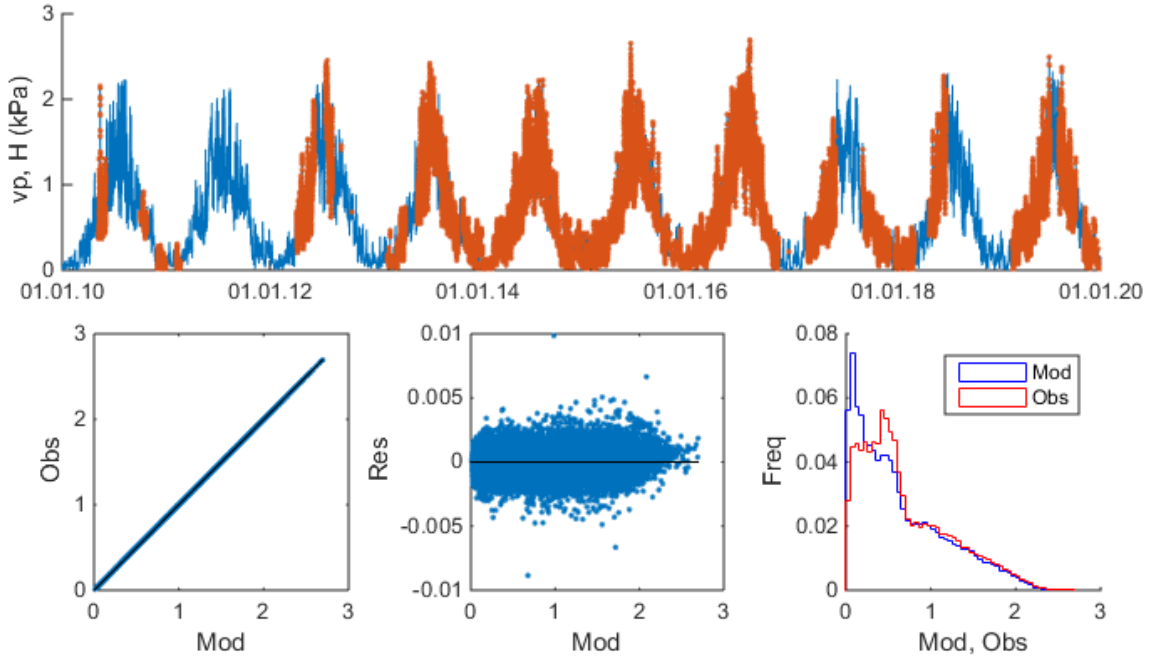

Figure S3. Water vapour pressure at the hollow at the MFS. See legend at Fig. S1.

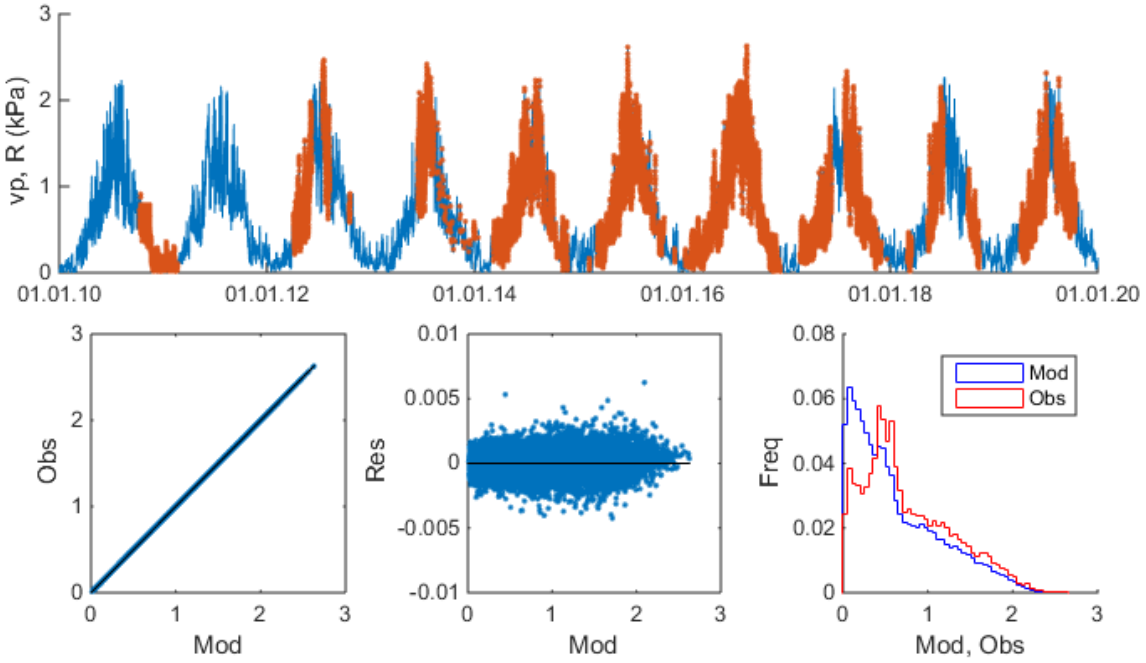

Figure S4. Water vapour pressure at the ridge at the MFS. See legend at Fig. S1.

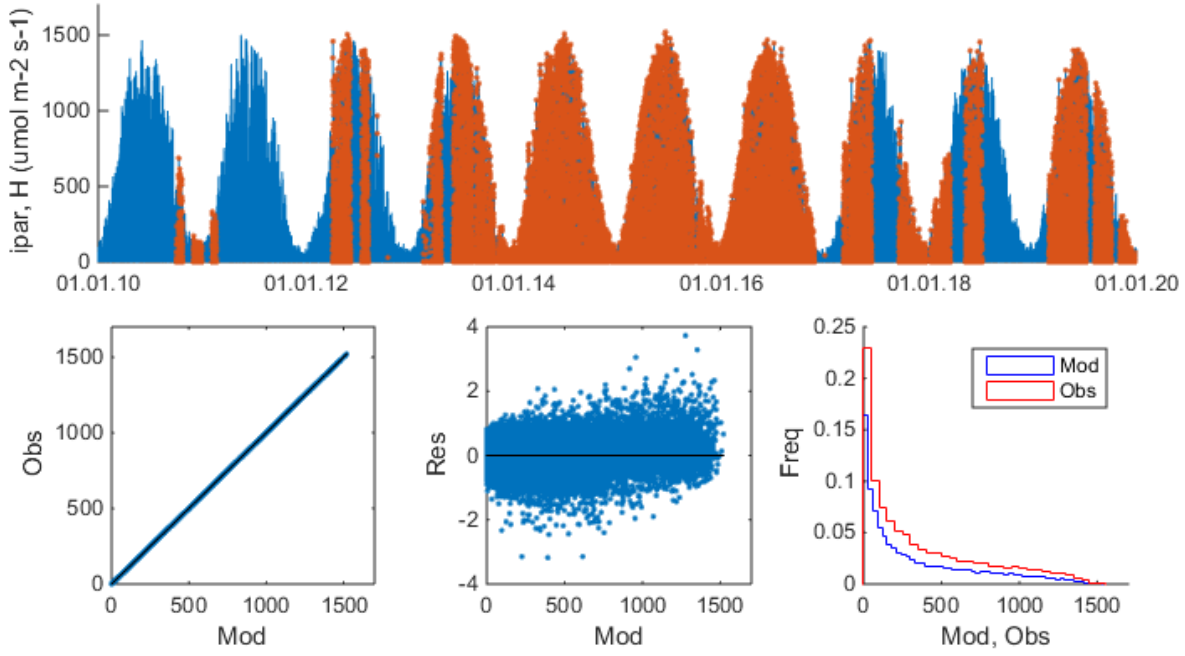

Figure S5. Incoming photosynthetically active radiation at the hollow at the MFS. See legend at Fig. S1.

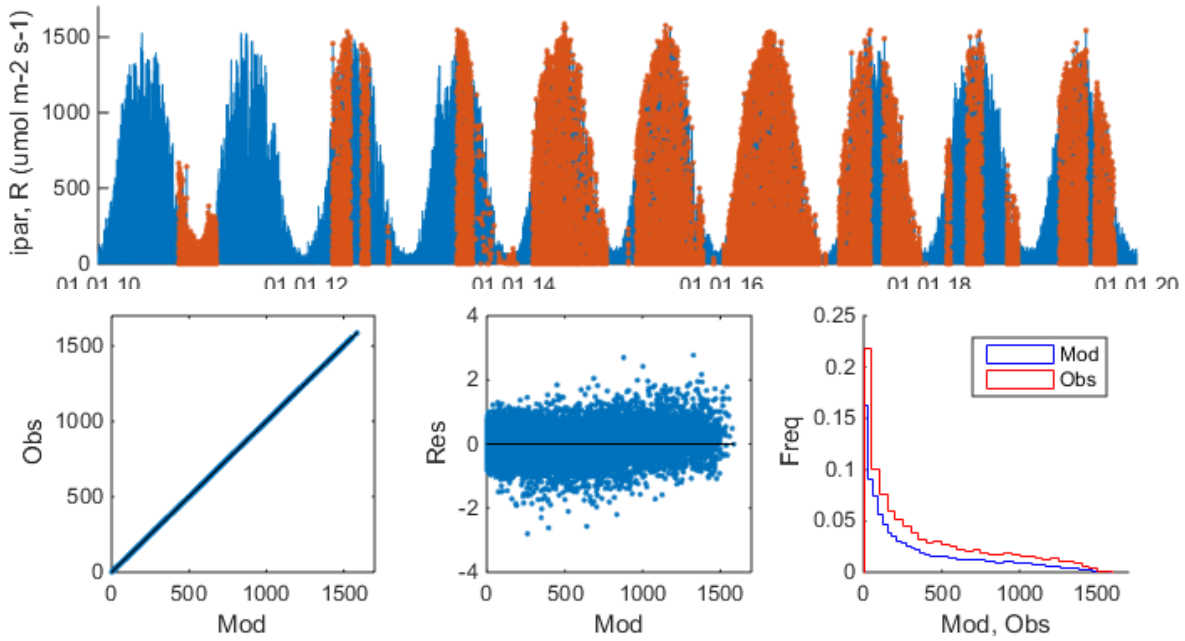

Figure S6. Incoming photosynthetically active radiation at the ridge at the MFS. See legend at Fig. S1.

25

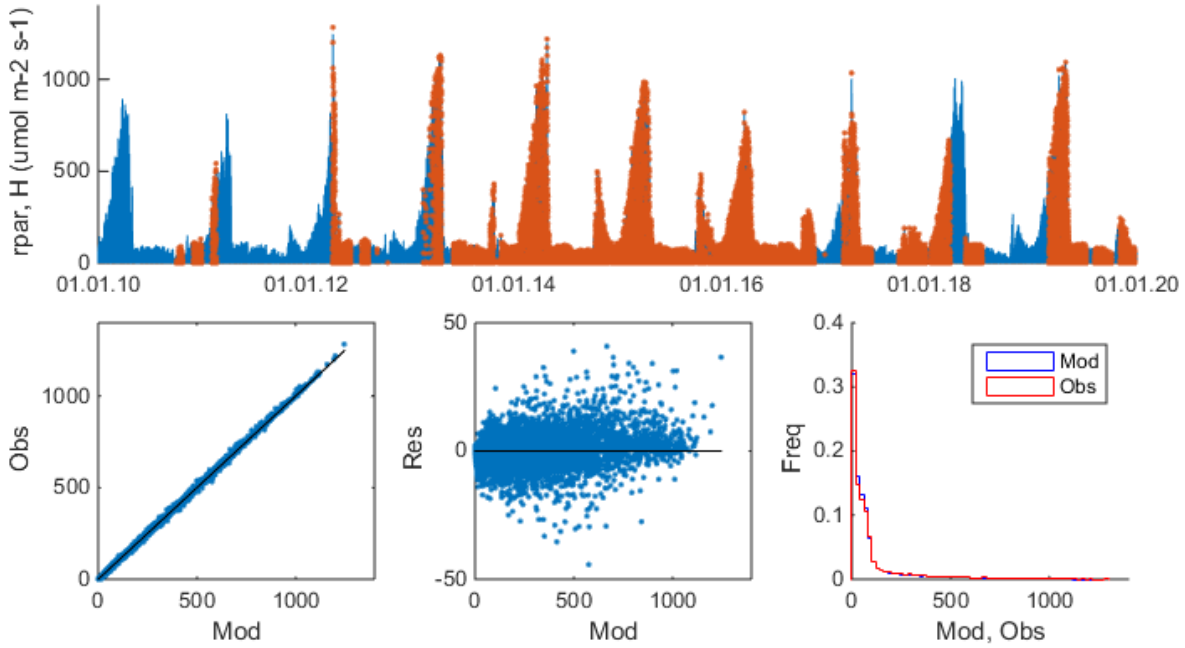

Figure S7. Reflected photosynthetically active radiation at the hollow at the MFS. See legend at Fig. S1.

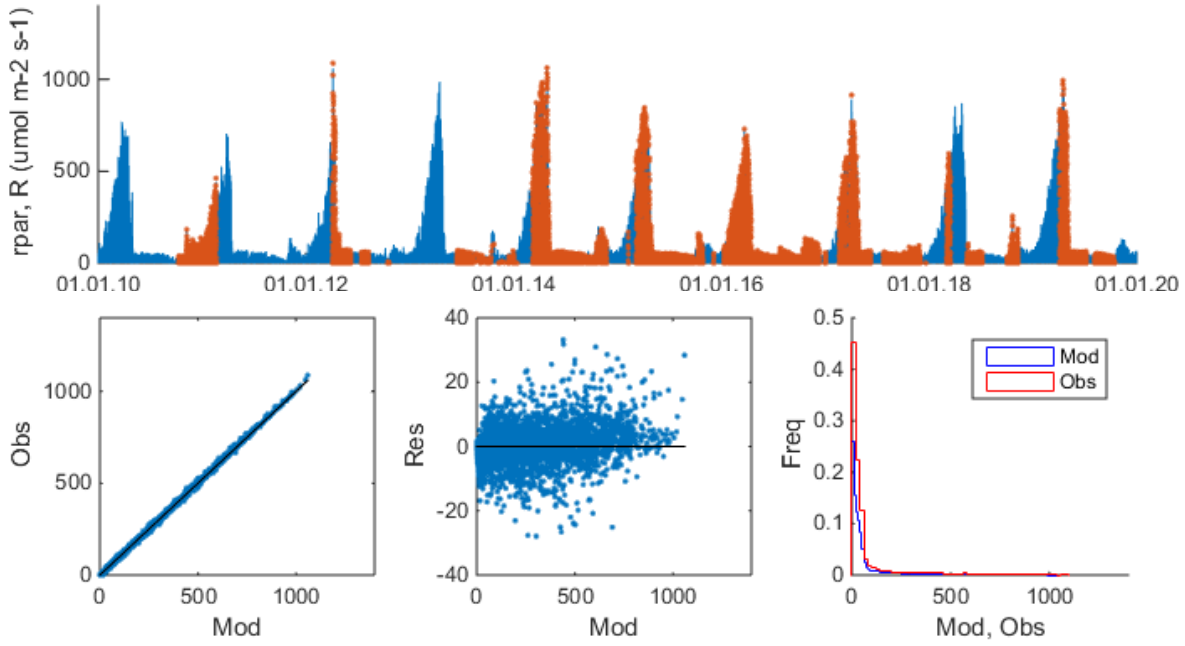

Figure S8. Reflected photosynthetically active radiation at the ridge at the MFS. See legend at Fig. S1.

30

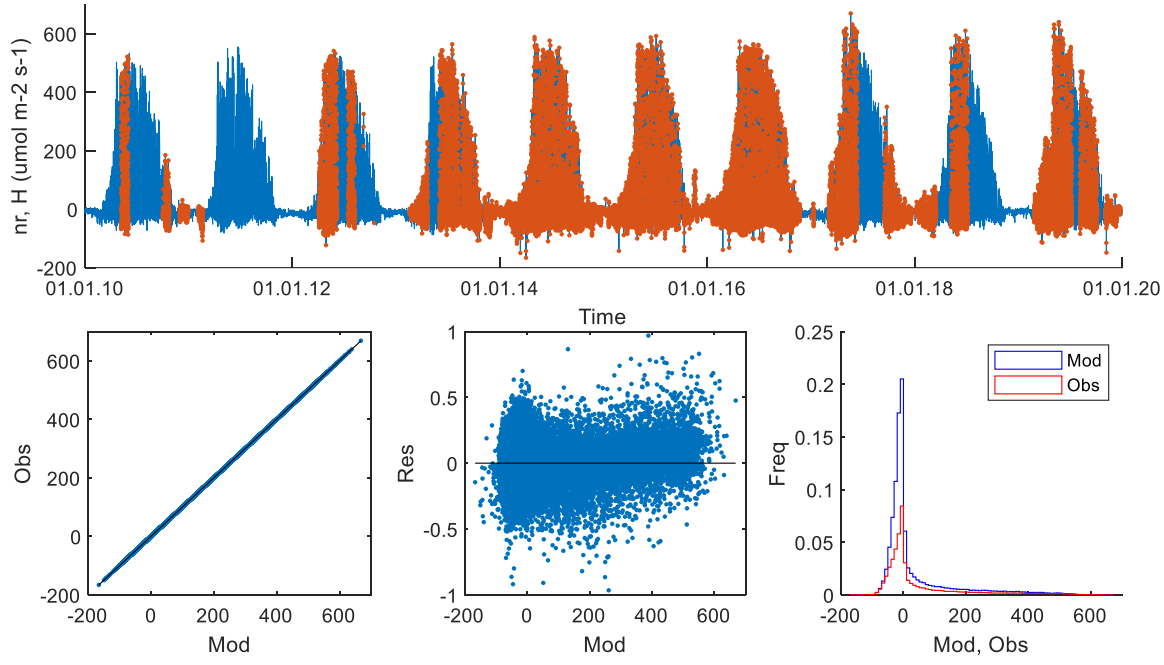

Figure S9. Net radiation balance at the hollow at the MFS. See legend at Fig. S1.

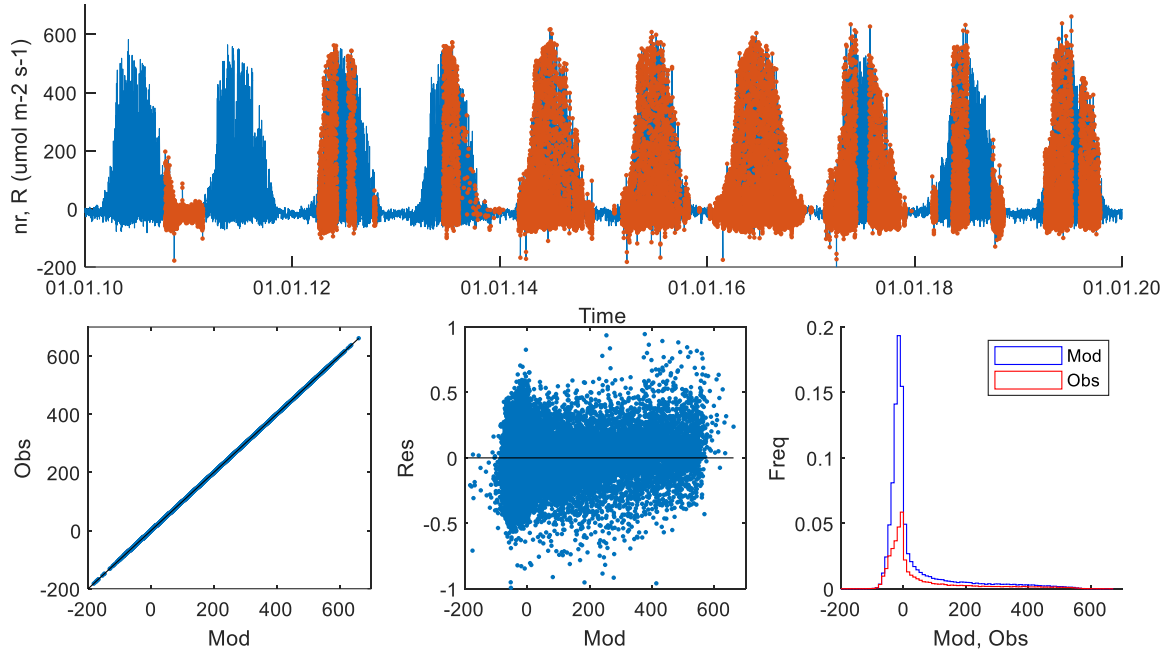

35 **Figure S10. Net radiation balance at the ridge at the MFS. See legend at Fig. S1.**

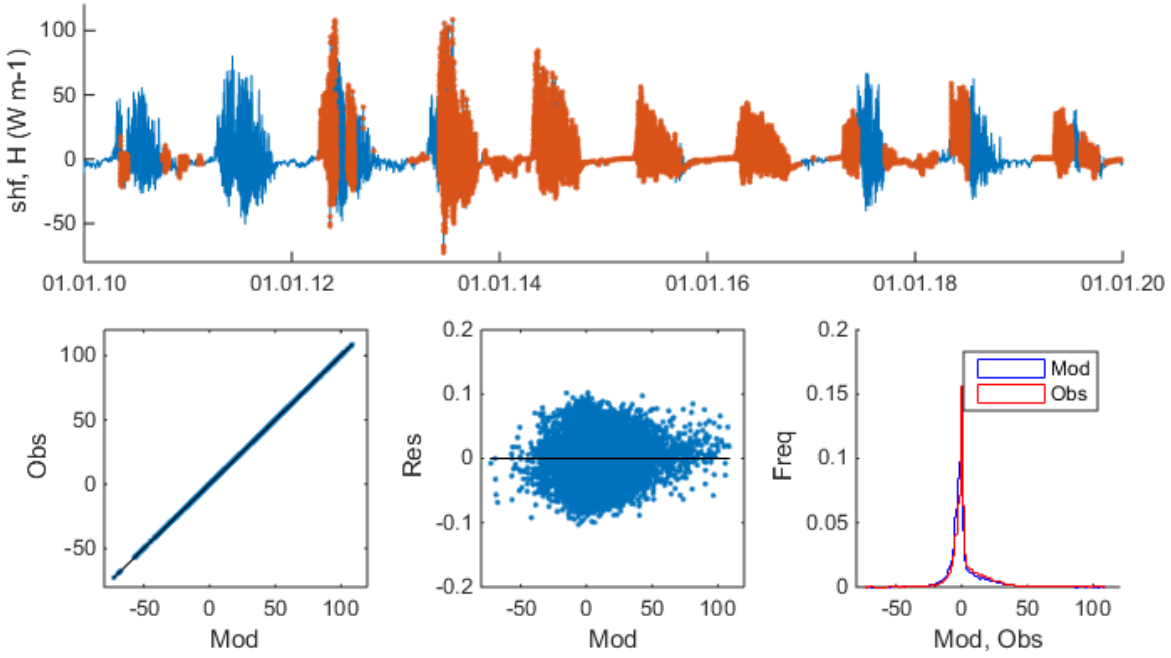

Figure S11. Soil heat flux at the hollow at the MFS. See legend at Fig. S1.

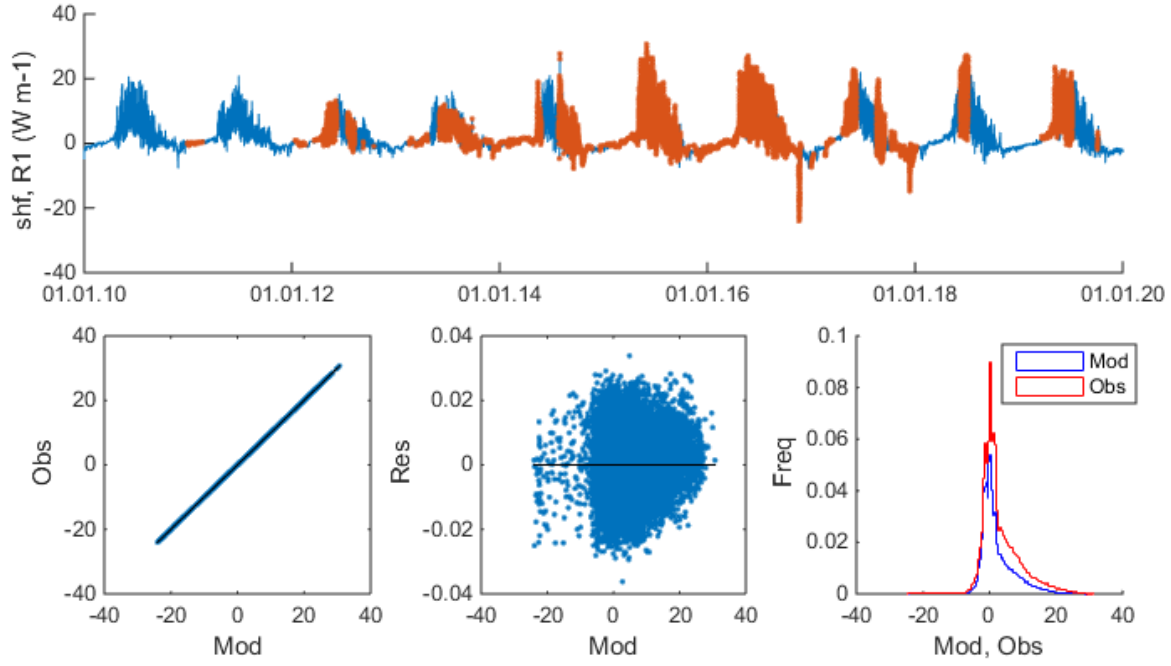

Figure S12. Soil heat flux at the ridge (site 1) at the MFS. See legend at Fig. S1.

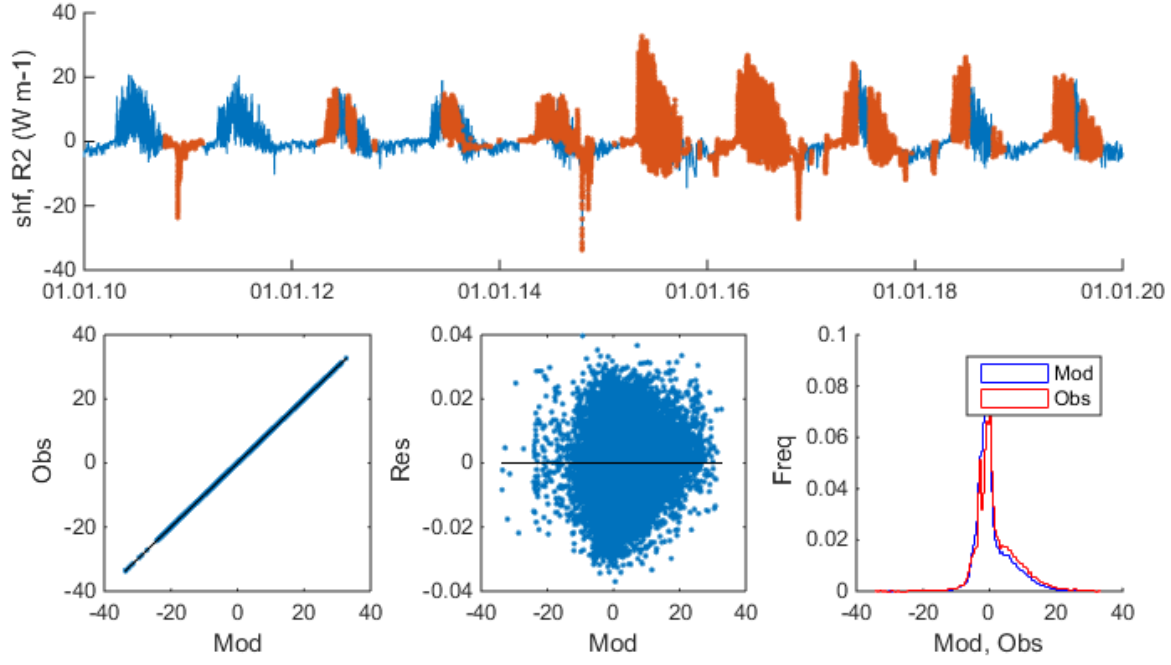

Figure S13. Soil heat flux at the ridge (site 2) at the MFS. See legend at Fig. S1.

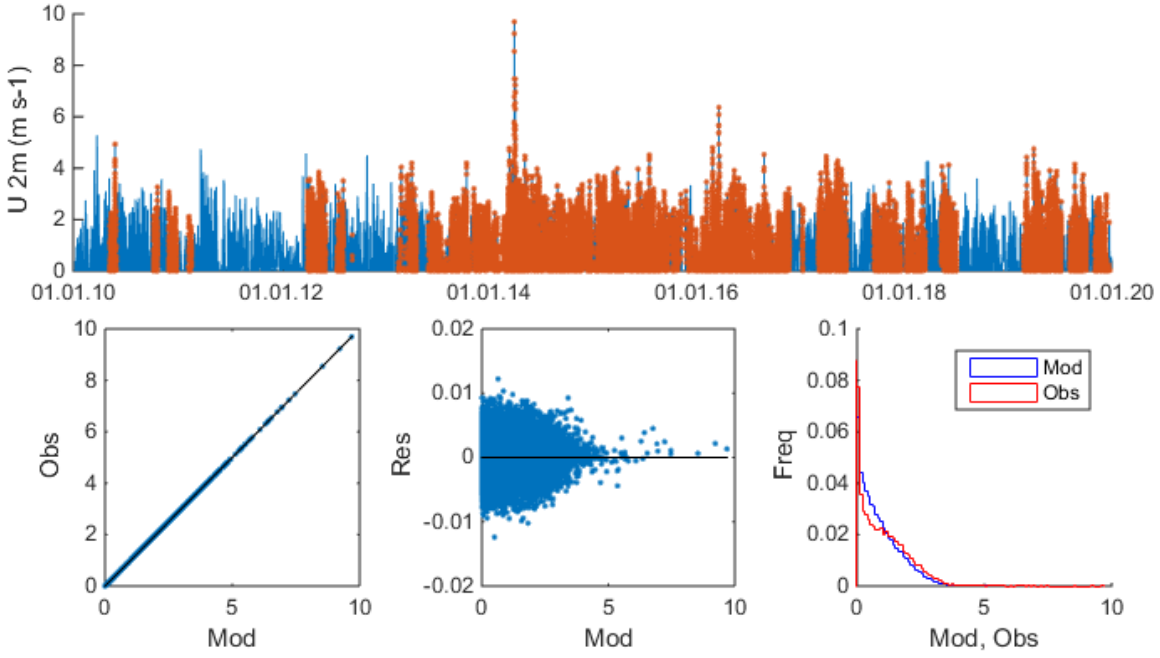

Figure S14. U-wind component at 2 m above the hollow surface at the MFS. See legend at Fig. S1.

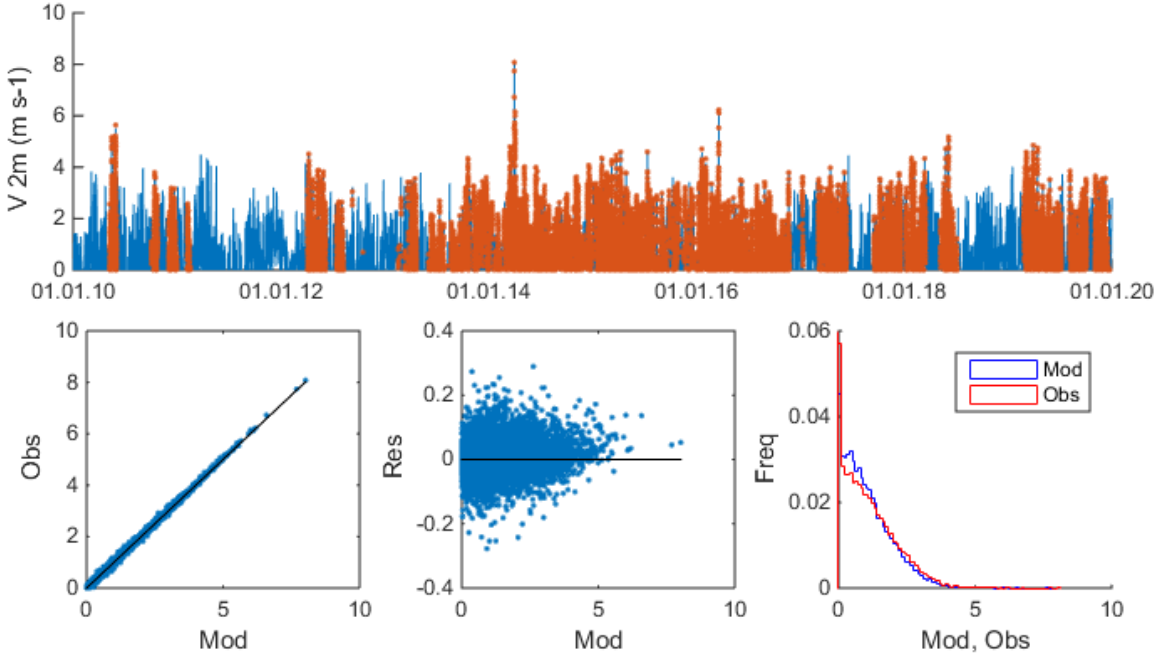

Figure S15. V-wind component at 2 m above the hollow surface at the MFS. See legend at Fig. S1.

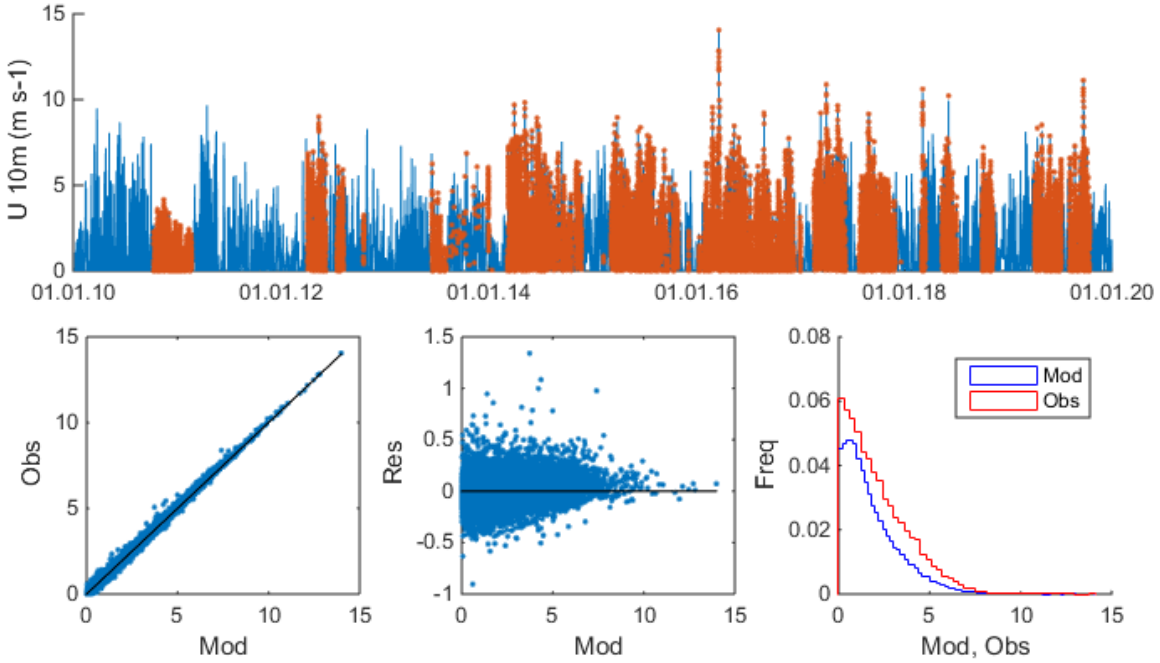

Figure S16. U-wind component at 10 m above the ridge surface at the MFS. See legend at Fig. S1.

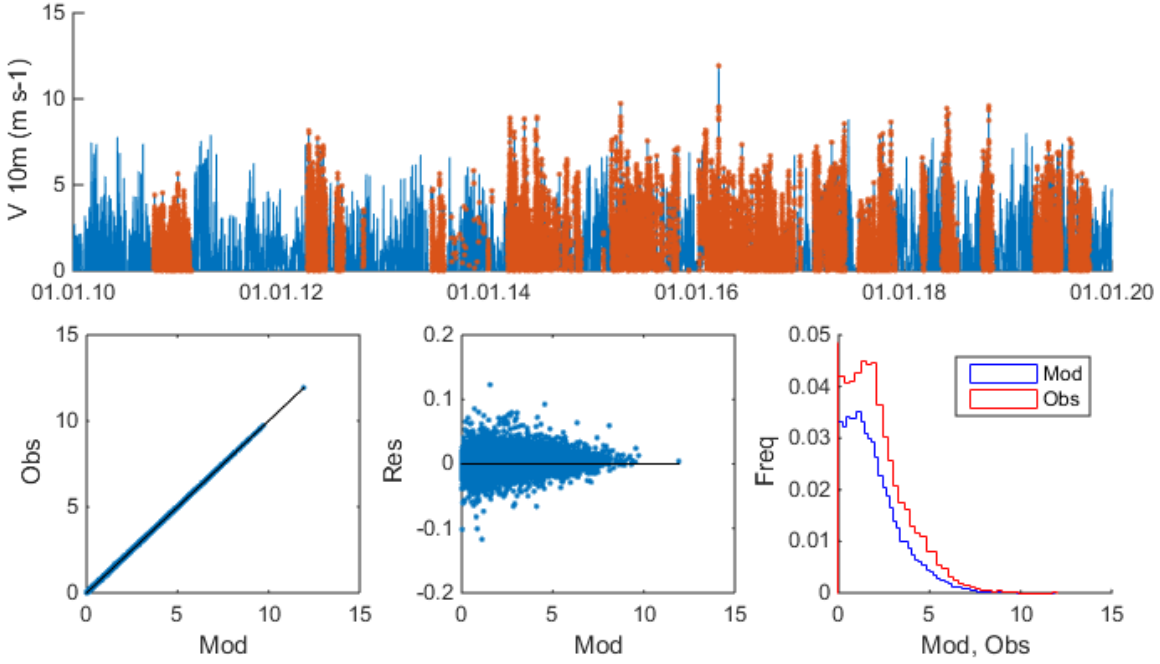

Figure S17. V-wind component at 10 m above the ridge surface at the MFS. See legend at Fig. S1.

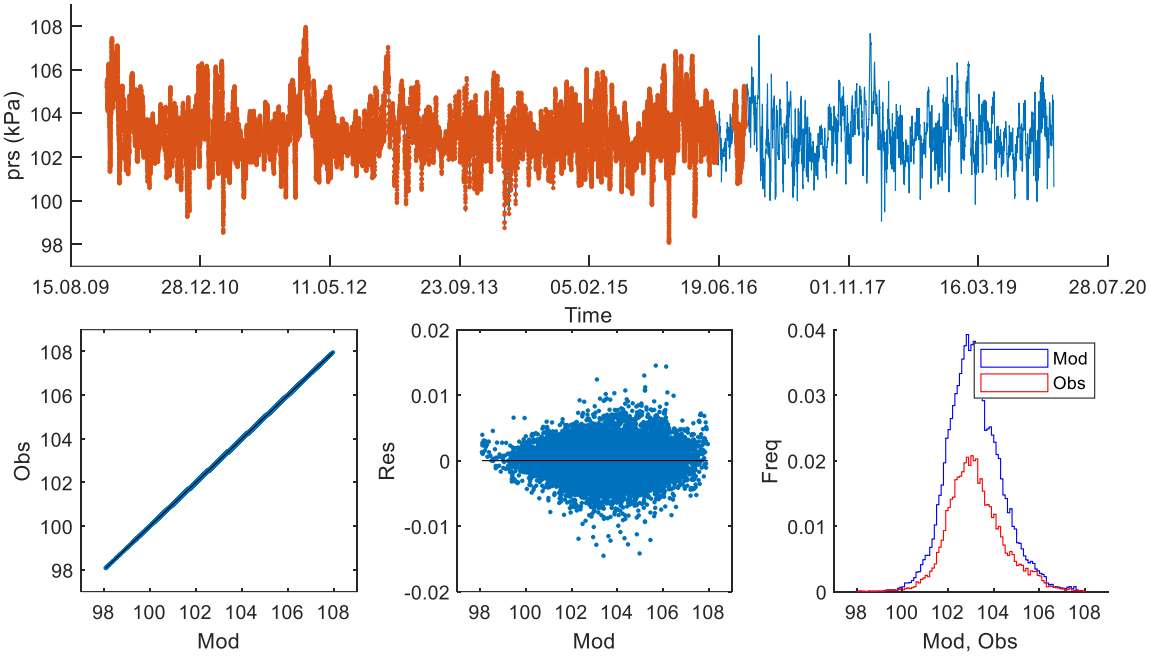

Figure S18. Atmospheric pressure at the MFS. See legend at Fig. S1.

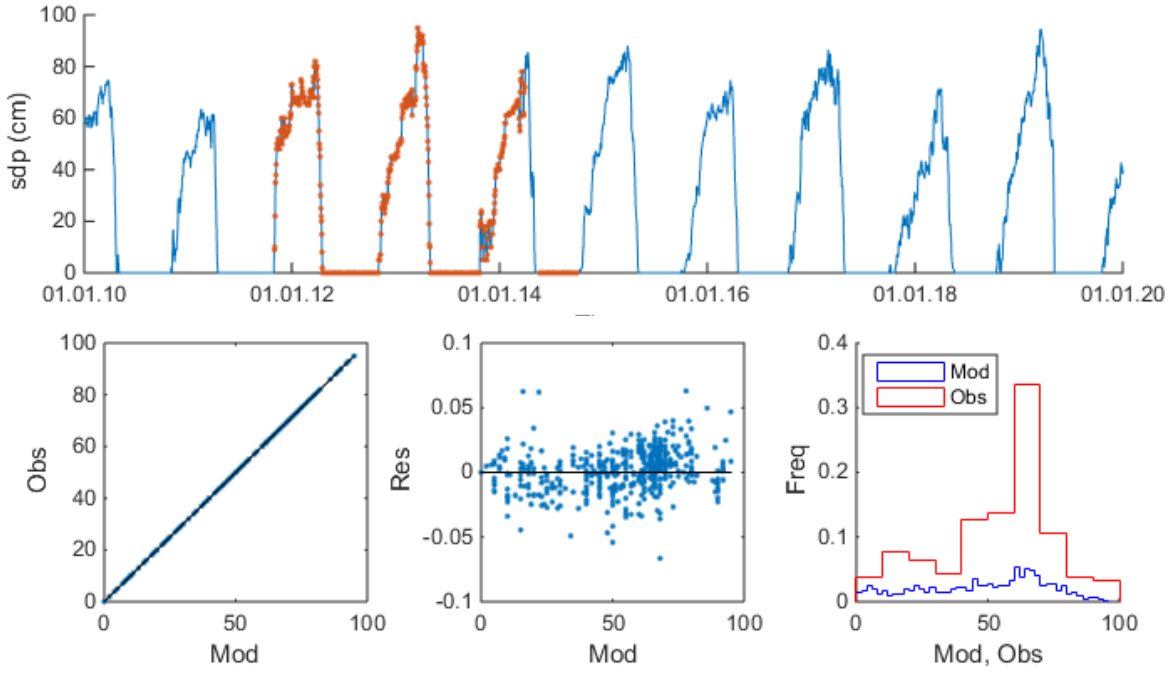

60

Figure S19. Snow depth at the hollow at the MFS. See legend at Fig. S1.

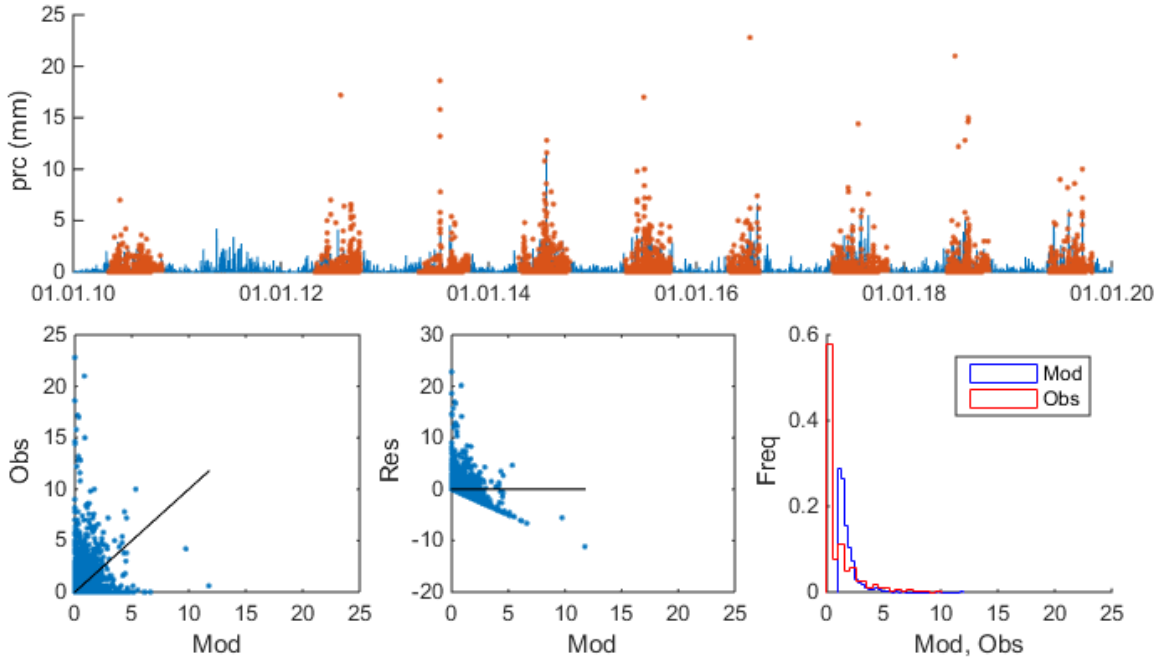

Figure S20. Liquid precipitations at the MFS. Top panel: 1 – hourly observations using rain gauge, 2 – ERA5-Land reanalysis data. Bottom panel: relations of observed and ERA5-Land data (left), difference of ERA5-Land with observation data (centre), frequency distributions for ERA5-Land and observed data (right).

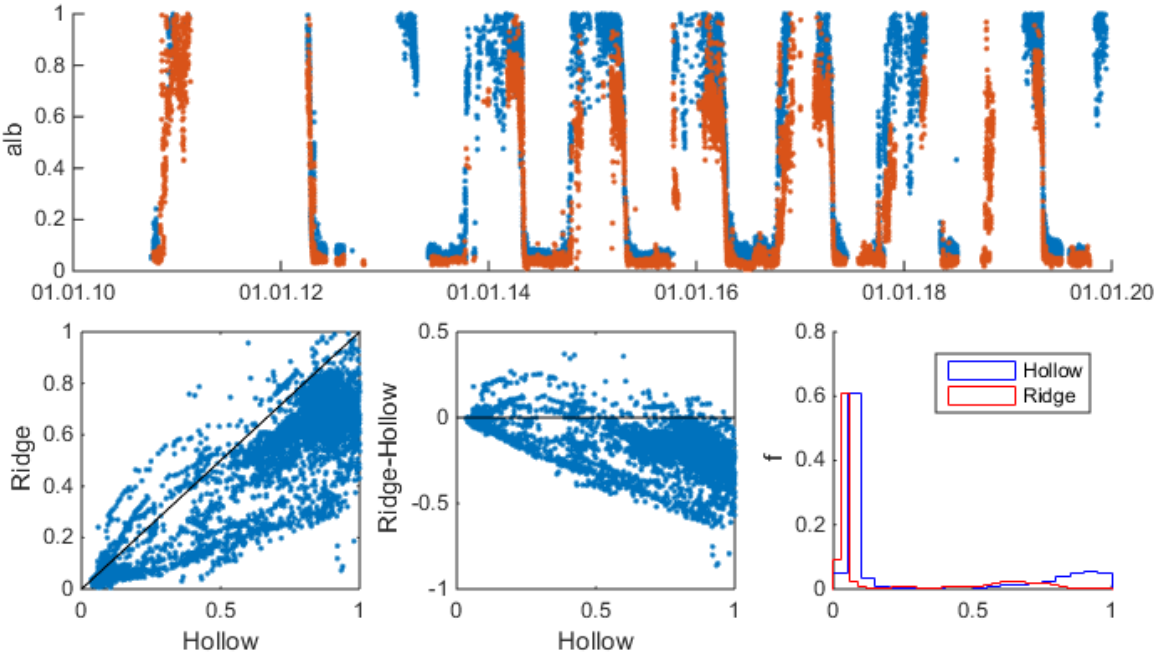

Figure S21. Albedo calculated from observations of incoming and reflected PAR at the MFS. Top panel: 1 – hollow, 2 – ridge. Bottom panel: data relations (left), difference of albedo at two sites (centre), frequency distributions (right).